

Figure 6 Correlation of neocortical ^{18}F -THK5105 and ^{11}C -PiB SUVR with MMSE scores (*upper*) and CDR-SOB scores (*lower*). Data from eight healthy control subjects (open circles) and eight patients with Alzheimer's disease (AD, filled circles) are shown.

of tau pathology (Soto, 2012; Mohamed *et al.*, 2013) from temporal areas to the other association cortices. A longitudinal assessment of tau pathology will help elucidate the spatial patterns of tau pathology progression in the living brain. In addition, as observed in ^{18}F -T807 and ^{18}F -T808 PET studies (Chien *et al.*, 2013, 2014), ^{18}F -THK5105 retention in the mesial temporal area was relatively lower than in the lateral temporal area in patients with Alzheimer's disease, which conflicts with microscopic observations showing higher neurofibrillary tangle density in the entorhinal cortex and hippocampus of Alzheimer's disease brain compared to the neocortex (Arnold *et al.*, 1991). One possible explanation for this phenomenon is the partial volume effect of radiotracer signals (Muller-Gartner *et al.*, 1992). ^{18}F -THK5105 retention in the mesial temporal cortex might be underestimated in patients with severe hippocampal atrophy.

^{18}F -THK5105 retention in patients with Alzheimer's disease was closely associated with dementia severity. This finding is consistent with results from previous post-mortem studies showing significant correlations of neurofibrillary tangle density with dementia severity (Arriagada *et al.*, 1992; Bierer *et al.*, 1995; Berg *et al.*, 1998). Our results further demonstrate that hippocampal atrophy is significantly correlated with ^{18}F -THK5105 retention but not with ^{11}C -PiB retention in the same area. In addition, the neocortical grey matter volume was negatively correlated with global ^{18}F -THK5105 retention in the neocortex. These findings

correspond with the neuropathological observation that the density of neurofibrillary tangles, but not senile plaques, is closely associated with neuronal loss (Gomez-Isla *et al.*, 1996, 1997). Intriguingly, ^{18}F -THK5105 retention in healthy control subjects was significantly higher in the mesial temporal cortex (SUVR = 1.17) than in the neocortex (SUVR = 1.05). This finding is likely to reflect age-related tau accumulation in this area. In future studies, the association of mesial temporal ^{18}F -THK5105 retention with ageing should be evaluated in a large population. It is also still unclear whether or not tau accumulation precedes neuronal loss. To answer this question, mesial temporal cortex tau density should be evaluated in the mild cognitive impairment population, as well as cognitively normal individuals with amyloid- β deposition, and these results should be compared with fluorodeoxyglucose and brain atrophy in a longitudinal analysis.

The amount of neocortical ^{18}F -THK5105 retention (SUVR = 1.23) was considerably lower than that of ^{11}C -PiB (SUVR = 2.75) in patients with Alzheimer's disease. This is thought to result from higher concentrations of amyloid- β fibrils than tau fibrils in the Alzheimer's disease brain (Villemagne *et al.*, 2012). Therefore, a tau-specific radiotracer must be highly sensitive and selective to tau protein fibrils. Our previous study demonstrated that the binding affinity of ^{18}F -THK5105 for tau fibrils (K_d = 1.45 nM) was 25-times higher than to amyloid- β fibrils (K_d = 35.9 nM) (Okamura *et al.*, 2013). Autoradiography studies

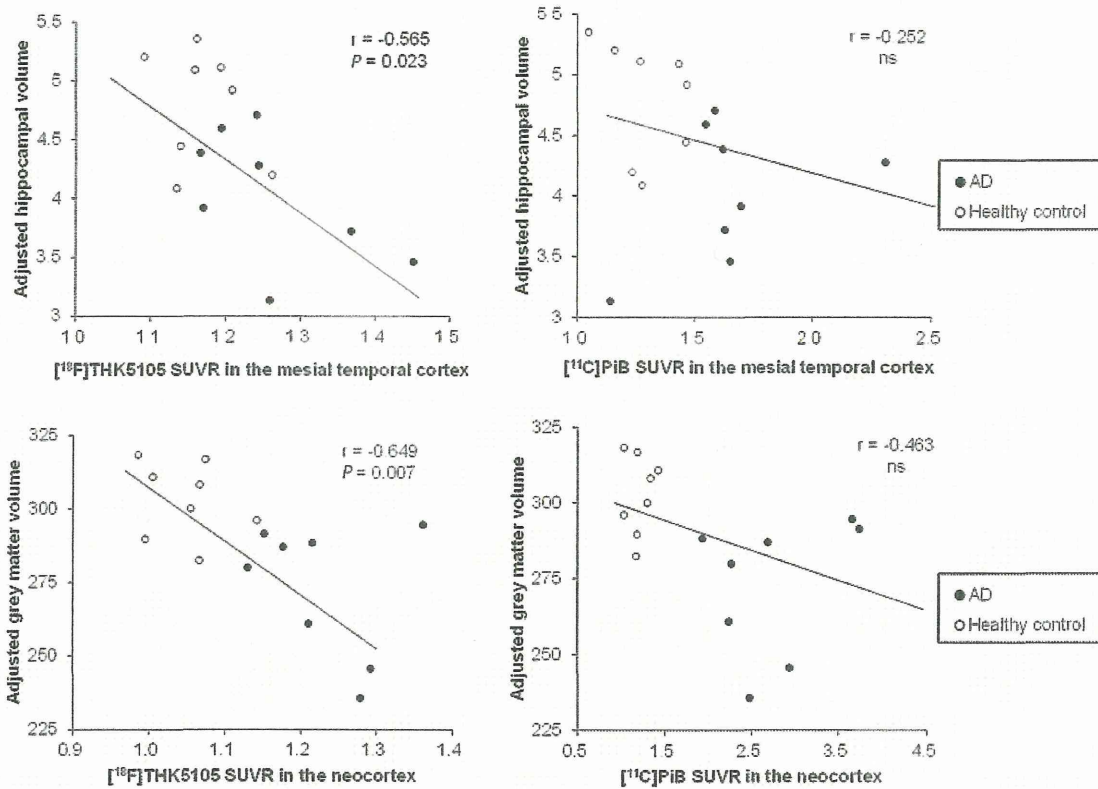


Figure 7 Correlation of ^{18}F -THK5105 and ^{11}C -PiB SUVR with adjusted hippocampal volumes (*upper*) or grey matter volumes (*lower*). Data from eight healthy control subjects (open circles) and eight patients with Alzheimer's disease (AD, filled circles) are shown.

further confirmed the preferential binding ability of ^{18}F -THK5105 to tau protein deposits in Alzheimer's disease brain sections. In this PET study, all Alzheimer's disease cases were PiB-positive and showed remarkable PiB retention in broad neocortical areas. As reported by many researchers, these patients with Alzheimer's disease showed prominent PiB retention in the ventrolateral prefrontal cortex (SUVR > 2.0), reflecting high amyloid- β pathology in this area. In contrast, ^{18}F -THK5105 retention in the frontal cortex was not elevated in more than half of the Alzheimer's disease cases (Fig. 4). In addition, one healthy control case showing PiB retention in the frontal cortex showed no retention of ^{18}F -THK5105 in this area. These results support the low sensitivity of ^{18}F -THK5105 to amyloid- β plaques.

Compared with previous ^{18}F -THK523 PET data, specific ^{18}F -THK5105 retention in grey matter was considerably higher whereas white matter retention was considerably lower than those observed for ^{18}F -THK523. This observation is consistent with previous *in vitro* autoradiograms showing a higher signal-to-background ratio of ^{18}F -THK5105 than ^{18}F -THK523 in Alzheimer's disease brain sections (Okamura *et al.*, 2013). This is probably due to the higher binding affinity of ^{18}F -THK5105 to tau protein fibrils. The peak brain entry of ^{18}F -THK5105 (cerebellar SUV = 4.5), which was observed before 6 min post-injection, was higher than for ^{18}F -THK523 and other reported radiotracers (^{18}F -T807, ^{18}F -T808 and ^{11}C -PBB3) and almost identical to the

reported SUV value of ^{11}C -PiB (Klunk *et al.*, 2004). In addition, ^{18}F -THK5105 did not accumulate in the skull, which is often the result of defluorination and interferes with visual PET image inspection. These pharmacokinetic properties are unique advantages of ^{18}F -THK5105 over the other reported radiotracers. Conversely, one of the drawbacks of ^{18}F -THK5105 is the existence of non-specific tracer retention in the brainstem, thalamus, and subcortical white matter, which reflects the binding of tracer to β -sheet structures present in myelin basic protein, similar to that observed for ^{11}C -PiB (Stankoff *et al.*, 2011). Nevertheless, the ^{18}F -THK5105 signal in the subcortical white matter was not visually noticeable as compared with ^{18}F -THK523 and ^{11}C -PiB. The relatively slower kinetics of ^{18}F -THK5105 cause the high background signals in grey matter, which may make the white matter signals less noticeable. Actually, the clearance of ^{18}F -THK5105 from normal grey matter tissue was slower than that of PiB because of higher lipophilicity for ^{18}F -THK5105 (LogP = 3.03) than PiB (LogP = 1.20). As another tau-imaging radiotracer candidate, we have developed a 2-arylquinoline derivative named ^{18}F -THK5117 (Okamura *et al.*, 2013), which is more hydrophilic and shows faster pharmacokinetics in mice than ^{18}F -THK5105. It is expected to show faster clearance from normal brain tissue in humans and higher signal-to-background ratio than ^{18}F -THK5105. A clinical trial testing ^{18}F -THK5117 is currently underway.

Tau deposits are also present in non-Alzheimer's disease tauopathies including frontotemporal lobe degeneration, corticobasal degeneration, progressive supranuclear palsy and chronic traumatic encephalopathy. Although THK523 failed to detect tau deposits in these non-Alzheimer's disease tauopathies, we recently observed *in vitro* binding ability of THK5105 and THK5117 to glial tau pathology in corticobasal degeneration and progressive supranuclear palsy. Therefore, clinical PET study in non-Alzheimer's disease tauopathies will be necessary to decide whether ^{18}F -THK5105 is applicable to the study of a broad range of tauopathies.

The results of the current study indicate that ^{18}F -THK5105 has adequate safety to be used as a clinical PET tracer. ^{18}F -THK5105 PET demonstrated high tracer retention in sites susceptible to paired helical filament-tau deposition in patients with Alzheimer's disease and distinctly differentiated patients with Alzheimer's disease from age-matched healthy controls. Collectively, these findings suggest that ^{18}F -THK5105 is useful for the non-invasive evaluation of tau pathology in humans and could be employed to study longitudinal tau deposition in healthy and pathological ageing.

Acknowledgements

We thank Prof. Michael Woodward, Dr John Merory, Dr Gordon Chan, Dr Kenneth Young, Dr David Darby, Ms Fiona Lamb, and the Brain Research Institute for their assistance with this study.

Funding

This study was supported by the research fund from GE Healthcare, the SEI (Sumitomo Electric Industries, Ltd) Group CSR Foundation, NHMRC grant 1044361 and NIRG grant from the Alzheimer's Association, the Industrial Technology Research Grant Program of the New Energy and Industrial Technology Development Organization (NEDO) in Japan (09E51025a), Health and Labor Sciences Research Grants from the Ministry of Health, Labor, and Welfare of Japan, Grant-in-Aid for Scientific Research (B) (23390297) and "Japan Advanced Molecular Imaging Program (J-AMP)" of the Ministry of Education, Culture, Sports, Science and Technology (MEXT), Japan.

References

- Abner EL, Kryscio RJ, Schmitt FA, Santacruz KS, Jicha GA, Lin Y, et al. "End-stage" neurofibrillary tangle pathology in preclinical Alzheimer's disease: fact or fiction? *J Alzheimers Dis* 2011; 25: 445–53.
- Arnold SE, Hyman BT, Flory J, Damasio AR, Van Hoesen GW. The topographical and neuroanatomical distribution of neurofibrillary tangles and neuritic plaques in the cerebral cortex of patients with Alzheimer's disease. *Cereb Cortex* 1991; 1: 103–16.
- Arriagada PV, Growdon JH, Hedley-Whyte ET, Hyman BT. Neurofibrillary tangles but not senile plaques parallel duration and severity of Alzheimer's disease. *Neurology* 1992; 42: 631–9.
- Berg L, McKeel DW Jr, Miller JP, Baty J, Morris JC. Neuropathological indexes of Alzheimer's disease in demented and nondemented persons aged 80 years and older. *Arch Neurol* 1993; 50: 349–58.
- Berg L, McKeel DW Jr, Miller JP, Storandt M, Rubin EH, Morris JC, et al. Clinicopathologic studies in cognitively healthy aging and Alzheimer's disease: relation of histologic markers to dementia severity, age, sex, and apolipoprotein E genotype. *Arch Neurol* 1998; 55: 326–35.
- Bierer LM, Hof PR, Purohit DP, Carlin L, Schmeidler J, Davis KL, et al. Neocortical neurofibrillary tangles correlate with dementia severity in Alzheimer's disease. *Arch Neurol* 1995; 52: 81–8.
- Bouras C, Hof PR, Giannakopoulos P, Michel JP, Morrison JH. Regional distribution of neurofibrillary tangles and senile plaques in the cerebral cortex of elderly patients: a quantitative evaluation of a one-year autopsy population from a geriatric hospital. *Cereb Cortex* 1994; 4: 138–50.
- Braak H, Braak E. Neuropathological staging of Alzheimer-related changes. *Acta Neuropathol* 1991; 82: 239–59.
- Checn DT, Bahri S, Szardenings AK, Walsh JC, Mu F, Su MY, et al. Early clinical PET imaging results with the novel PHF-tau radioligand [F-18]-T807. *J Alzheimers Dis* 2013; 34: 457–68.
- Chien DT, Szardenings AK, Bahri S, Walsh JC, Mu FR, Xia CF, et al. Early Clinical PET Imaging Results with the Novel PHF-Tau Radioligand [F18]-T808. *J Alzheimers Dis* 2014; 38: 171–84.
- Fodero-Tavoletti MT, Okamura N, Furumoto S, Mulligan RS, Connor AR, McLean CA, et al. 18F-THK523: a novel *in vivo* tau imaging ligand for Alzheimer's disease. *Brain* 2011; 134: 1089–100.
- Gomez-Isla T, Hollister R, West H, Mui S, Growdon JH, Petersen RC, et al. Neuronal loss correlates with but exceeds neurofibrillary tangles in Alzheimer's disease. *Ann Neurol* 1997; 41: 17–24.
- Gomez-Isla T, Price JL, McKeel DW Jr, Morris JC, Growdon JH, Hyman BT. Profound loss of layer II entorhinal cortex neurons occurs in very mild Alzheimer's disease. *J Neurosci* 1996; 16: 4491–500.
- Grundke-Iqbal I, Iqbal K, Quinlan M, Tung YC, Zaidi MS, Wisniewski HM. Microtubule-associated protein tau. A component of Alzheimer paired helical filaments. *J Biol Chem* 1986a; 261: 6084–9.
- Grundke-Iqbal I, Iqbal K, Tung YC, Quinlan M, Wisniewski HM, Binder LI. Abnormal phosphorylation of the microtubule-associated protein tau (tau) in Alzheimer cytoskeletal pathology. *Proc Natl Acad Sci USA* 1986b; 83: 4913–7.
- Harada R, Okamura N, Furumoto S, Tago T, Maruyama M, Higuchi M, et al. Comparison of the binding characteristics of [^{18}F]THK-523 and other amyloid imaging tracers to Alzheimer's disease pathology. *Eur J Nucl Med Mol Imaging* 2013; 40: 125–32.
- Harada R, Okamura N, Furumoto S, Yoshikawa T, Arai H, Yanai K, et al. Use of a benzimidazole derivative BF-188 in fluorescence multispectral imaging for selective visualization of tau protein fibrils in the Alzheimer's disease brain. *Mol Imaging Biol* 2014; 16: 19–27.
- Haroutunian V, Purohit DP, Perl DP, Marin D, Khan K, Lantz M, et al. Neurofibrillary tangles in nondemented elderly subjects and mild Alzheimer disease. *Arch Neurol* 1999; 56: 713–8.
- Klunk WE, Engler H, Nordberg A, Wang Y, Blomqvist G, Holt DP, et al. Imaging brain amyloid in Alzheimer's disease with Pittsburgh Compound-B. *Ann Neurol* 2004; 55: 306–19.
- Lee VM, Balin BJ, Otvos L Jr, Trojanowski JQ. A68: a major subunit of paired helical filaments and derivatized forms of normal Tau. *Science* 1991; 251: 675–8.
- Maruyama M, Shimada H, Suhara T, Shinotoh H, Ji B, Maeda J, et al. Imaging of tau pathology in a tauopathy mouse model and in Alzheimer patients compared to normal controls. *Neuron* 2013; 79: 1094–108.
- Masters CL, Cappai R, Barnham KJ, Villemagne VL. Molecular mechanisms for Alzheimer's disease: implications for neuroimaging and therapeutics. *J Neurochem* 2006; 97: 1700–25.
- Mintun MA, Larossa GN, Sheline YI, Dence CS, Lee SY, Mach RH, et al. [^{11}C]PIB in a nondemented population: potential antecedent marker of Alzheimer disease. *Neurology* 2006; 67: 446–52.
- Mohamed NV, Herrou T, Plouffe V, Piperno N, Leclerc N. Spreading of tau pathology in Alzheimer's disease by cell-to-cell transmission. *Eur J Neurosci* 2013; 37: 1939–48.

- Muller-Gartner HW, Links JM, Prince JL, Bryan RN, McVeigh E, Leal JP, et al. Measurement of radiotracer concentration in brain gray matter using positron emission tomography: MRI-based correction for partial volume effects. *J Cereb Blood Flow Metab* 1992; 12: 571–83.
- Okamura N, Furumoto S, Harada R, Tago T, Yoshikawa T, Fodero-Tavoletti M, et al. Novel 18F-labeled arylquinoline derivatives for non-invasive imaging of tau pathology in Alzheimer disease. *J Nucleic Med* 2013; 54: 1420–7.
- Okamura N, Suemoto T, Furumoto S, Suzuki M, Shimadzu H, Akatsu H, et al. Quinoline and benzimidazole derivatives: candidate probes for *in vivo* imaging of tau pathology in Alzheimer's disease. *J Neurosci* 2005; 25: 10857–62.
- Price JL, McKeel DW Jr, Buckles VD, Roe CM, Xiong C, Grundman M, et al. Neuropathology of nondemented aging: presumptive evidence for preclinical Alzheimer disease. *Neurobiol Aging* 2009; 30: 1026–36.
- Rowe CC, Ng S, Ackermann U, Gong SJ, Pike K, Savage G, et al. Imaging beta-amyloid burden in aging and dementia. *Neurology* 2007; 68: 1718–25.
- Shoghi-Jadid K, Small GW, Agdeppa ED, Kepe V, Ercoli LM, Siddarth P, et al. Localization of neurofibrillary tangles and beta-amyloid plaques in the brains of living patients with Alzheimer disease. *Am J Geriatr Psychiatry* 2002; 10: 24–35.
- Small GW, Kepe V, Ercoli LM, Siddarth P, Bookheimer SY, Miller KJ, et al. PET of brain amyloid and tau in mild cognitive impairment. *N Engl J Med* 2006; 355: 2652–63.
- Soto C. *In vivo* spreading of tau pathology. *Neuron* 2012; 73: 621–3.
- Sperling RA, Aisen PS, Beckett LA, Bennett DA, Craft S, Fagan AM, et al. Toward defining the preclinical stages of Alzheimer's disease: recommendations from the National Institute on Aging-Alzheimer's Association workgroups on diagnostic guidelines for Alzheimer's disease. *Alzheimers Dement* 2011; 7: 280–92.
- Stankoff B, Freeman L, Aigrot MS, Chardain A, Dolle F, Williams A, et al. Imaging central nervous system myelin by positron emission tomography in multiple sclerosis using [methyl-(1)(1)C]-2-(4'-methylamino-phenyl)-6-hydroxybenzothiazole. *Ann Neurol* 2011; 69: 673–80.
- Villemagne VL, Furumoto S, Fodero-Tavoletti MT, Harada R, Mulligan RS, Kudo Y, et al. The challenges of tau imaging. *Future Neurol* 2012; 7: 409–21.
- Villemagne VL, Pike KE, Chetelat G, Ellis KA, Mulligan RS, Bourgeat P, et al. Longitudinal assessment of Abeta and cognition in aging and Alzheimer disease. *Ann Neurol* 2011; 69: 181–92.
- Vos SJ, Xiong C, Visser PJ, Jasielec MS, Hassenstab J, Grant EA, et al. Preclinical Alzheimer's disease and its outcome: a longitudinal cohort study. *Lancet Neurol* 2013; 12: 957–65.

Received 3 July 2013,

Revised 31 August 2013,

Accepted 8 September 2013

Published online 16 October 2013 in Wiley Online Library

(wileyonlinelibrary.com) DOI: 10.1002/jlcr.3133

Synthesis and preliminary evaluation of 2-arylhydroxyquinoline derivatives for tau imaging

Tetsuro Tago,^a Shozo Furumoto,^{a,b,*} Nobuyuki Okamura,^b Ryuichi Harada,^b Yoichi Ishikawa,^a Hiroyuki Arai,^c Kazuhiko Yanai,^b Ren Iwata,^a and Yukitsuka Kudo^d

Alzheimer's disease (AD) is the most common cause of dementia. Senile plaques, consisting of β -amyloid, and neurofibrillary tangles (NFTs), composed of tau protein, are representative pathological hallmarks of AD. It is believed that the accumulation of NFTs precedes the onset of clinical symptoms of AD and correlates with the progression of memory dysfunction. Thus, the use of noninvasive detection techniques including radiolabeled probes and positron emission tomography (PET) will facilitate early diagnosis or staging of AD. In this study, we synthesized and evaluated novel hydroxylated 2-arylquinoline derivatives as tau imaging PET probes. The binding affinities of compounds for tau were evaluated by fluorescent staining of the AD hippocampal section and a competitive binding assay using [¹⁸F]THK-523. THK-951 showed high binding affinity for tau pathology in an AD brain section and K18 Δ 280K fibrils ($K_i = 20.7$ nM); thus, we radiosynthesized a ¹¹C-labeled THK-951 and further studied its potential as a tau PET probe. The [¹¹C]THK-951 demonstrated excellent kinetics in a normal mouse brain (3.23% ID/g at 2 min postinjection and 0.15% ID/g at 30 min postinjection) and showed the labeling of NFTs in an AD brain section by autoradiography assay. These findings indicate the availability of [¹¹C]THK-951 for in vivo PET imaging of tau pathology in AD.

Keywords: Alzheimer's disease; tau; positron emission tomography; imaging

Introduction

Alzheimer's disease (AD) is a typical neurodegenerative disorder associated with memory impairment, disorientation, and language disorder. Because AD shows complex and diverse clinical symptoms, which overlap with other dementias, its definitive diagnosis is reliant on postmortem examination rather than clinical diagnosis. Neuronal atrophy and deposition of senile plaques (SPs) and neurofibrillary tangles (NFTs) in the brain represent the pathological hallmarks of AD.^{1–3} Consequently, noninvasive imaging techniques to measure these pathological changes can be indispensable to the differential diagnosis of AD.

According to amyloid hypothesis, the AD pathogenic mechanism starts with the abnormal accumulation of SPs consisting of β -amyloid aggregation in the brain.⁴ With a view to presymptomatic diagnosis, investigation into the detection of lesions using positron emission tomography (PET) or single photon emission computed tomography has been promoted in this decade, and many radiolabeled ligands were developed ([¹⁸F]FDDNP,⁵ [¹¹C]PIB,⁶ [¹⁸F]JAV-45,⁷ [¹¹C]BF-227,⁸ and [¹²³I]/¹²⁵I]IMPY⁹).¹⁰ These ligands have been successful for the detection of SPs in living human brains and were useful for confirming the correlation between PET images and autopsy results.^{11–13}

Although β -amyloid PET imaging studies have high sensitivity and can detect SPs before clinical symptoms appear, they also showed that the association between $A\beta$ signals and acuteness of symptom was limited.^{4,14} Therefore, to estimate AD severity

from pathological changes, other quantitatively detectable biomarkers are desired.

Tau proteins, which associate with the stabilization of microtubules, are abnormally phosphorylated and form paired helical filaments (PHFs) in the AD patient's brain.^{15,16} PHFs finally assemble into NFTs, neuropil threads, and dystrophic neurites. Neurofibrillary lesions appear in certain brain areas before the onset of dementia, and autopsy studies indicate a higher association between tau pathology levels and cognitive dysfunction relative to $A\beta$ pathology.^{17–20} Thus, quantitative imaging of tau burden may serve to not only monitor the progression of neurodegeneration but also evaluate the therapeutic effect of longitudinal tau-targeted AD treatments.

^aCyclotron and Radioisotope Center (CYRIC), Tohoku University, Sendai 980-8578, Japan

^bDepartment of Pharmacology, Tohoku University School of Medicine, Sendai 980-8575, Japan

^cDepartment of Geriatrics & Gerontology, Institute of Development, Aging and Cancer, Tohoku University, Sendai 980-8575, Japan

^dInnovation of New Biomedical Engineering Center, Tohoku University, Sendai 980-8574, Japan

*Correspondence to: Shozo Furumoto, Cyclotron and Radioisotope Center (CYRIC), Tohoku University, 6-3 Aoba, Aramaki, Aoba-ku, Sendai 980-8578, Japan. E-mail: furumoto@cyric.tohoku.ac.jp

Recently, several tau ligands for PET or single photon emission computed tomography imaging have been reported.^{21,22} Kolb and colleagues have reported ¹⁸F-labeled tau tracers, [¹⁸F]T807 and [¹⁸F]T808, and these tracers showed promising results in both *in vitro* and *in vivo* studies.^{23–25} We have developed 2-arylquinoline derivatives with a preference to bind tau lesions rather than A β as previously reported.^{26,27} Through the structural optimization, we recently reported ¹⁸F-labeled derivatives [¹⁸F]THK-5105 and [¹⁸F]THK-5117.²⁸ They appear to have more preferable properties as a PET tau imaging radiotracer compared with [¹⁸F]THK-523.²⁷ The preliminary clinical studies using these tracers are currently in progress.

Lipophilic ligands display higher nonspecific binding; therefore, lower lipophilicity is important for ideal brain kinetics as brain imaging PET tracers. Low nonspecific binding contributes to high signal-to-background ratio and facilitates the visualization of lower burden of tau pathology. The aim of the present study was to develop a ¹¹C-labeled tau probe with fast clearance from nonspecific regions. We developed novel hydroxylated quinoline derivatives (Figure 1) with lower lipophilicity and evaluated their potential as tau probes for PET.

Experimental

Synthesis of 2-arylquinoline derivatives

Methods for the synthesis and characterization data of 2-arylquinoline derivatives (shown in Schemes 1 and 2) are described in detail in the Supporting Information.

Radiolabeling of [¹¹C]THK-951

[¹¹C]Methyl iodide was prepared from [¹¹C]carbon dioxide produced with a Cypris HM12 cyclotron (Sumitomo Heavy Industries Inc., Tokyo, Japan) by a catalytic iodination reaction via [¹¹C]methane (MeI MicroLab, GE Healthcare, Waukesha, WI, USA). [¹¹C]Methyl triflate ([¹¹C]MeOTf) used for radiolabeling was prepared from [¹¹C]methyl iodide by passing through a silver triflate-graphpac (Sigma-Aldrich, St Louis, USA) gas chromatography column heated at 200 °C. The compound **15** indicated in Scheme 2 was used as a radiolabeling precursor. The precursor (1.0 mg) and tBuOK (1.0 mg) were dissolved in dimethyl sulfoxide (DMSO) (400 μ L). [¹¹C]MeOTf was bubbled through the solution, followed by heating at 110 °C for 1 min. Then, 2N HCl (1 mL) was added to the solution, and it was heated at an additional 10 min at the same temperature. The solution was neutralized with 4N NaOH (0.5 mL), and the crude mixture was purified with semi-preparative HPLC using an Inertsil® ODS-3 (GL Sciences Inc., Tokyo, Japan) eluted with acetonitrile/20 mM NaH₂PO₄ (pH 4.8) (40/60, flow rate: 5.0 mL/min). The fraction containing [¹¹C]THK-951 was mixed with water (20 mL) and 25% ascorbic acid (0.5 mL) and passed through an activated Sep-Pak tC18 Plus (Waters, Milford, MA, USA). The Sep-Pak cartridge was washed with water, and then, [¹¹C]THK-951 was eluted with ethanol. The ethanol solution was used for the *in vitro* autoradiography (ARG) assay. For the *ex vivo* biodistribution study, ethanol was removed by evaporation, and the product was solubilized into saline with polysorbate 80 (<0.1%).

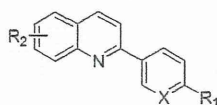


Figure 1. Chemical structure of hydroxyquinoline derivatives. Compounds in this study include the following: X = CH, N; R₁ = NH₂, NHCH₃; R₂ = 6-OH, 7-OH.

Measurement of logP values

The octanol/water partition coefficients of the tested compounds were estimated by HPLC method of the OECD (Organisation for Economic Co-operation and Development) guideline²⁹ according to the slightly modified procedures we recently reported.²⁸

In vitro fluorescent binding assay with tau fibrils

Preparation of K18 Δ 280K-tau fibrils

Recombinant K18 Δ 280K-tau was custom generated by Life Technologies Japan Ltd. (Tokyo, Japan). K18 Δ 280K-tau fibrils were prepared as described previously.^{27,30} Briefly, K18 Δ 280K-tau solution was diluted with phosphate buffered saline (pH 7.4) to a final concentration of 20 μ M. The solution was incubated at 37 °C for a day with agitation (1000 rpm). Fibril formation was confirmed by thioflavin-S fluorescence spectroscopy.

In vitro fluorescence binding assay

Synthetic K18 Δ 280K-tau fibrils (200 nM) were incubated with 3 μ M (THK-951 and THK-5272) or 5 μ M (THK-953 and THK-5273) compounds at room temperature for 1 h. The fluorescence intensity was measured at an excitation wavelength appropriate for each compound. The incubations were carried out on Nunc 96 MicroWell™ black plates (Nalge Nunc Int., Rochester, NY, USA), using 200 μ L of phosphate buffer saline (pH 7.4) as the reaction mixture. All experiments were conducted in triplicate.

In vitro neuropathological staining using brain sections

The staining properties of the tested compounds were examined using postmortem brain tissues from an autopsy-confirmed case of AD (82-year-old woman). The experiments were performed in accordance with the regulations of the ethics committee of Tohoku University. A series of 8 μ m thick sections from paraffin-embedded blocks of hippocampus were used for staining. According to the method reported previously,^{28,31} the sections were immunostained with anti-tau antibody (AT8; Innogenetics, Ghent, Belgium). Stained images were examined using an Olympus (Tokyo, Japan) BX51 microscope equipped with blue-violet (BP, 400–440; DM, 455; BA, 475) and blue filters (BP, 460–490; DM, 500; BA, 520IF).

Competitive binding assay with [¹⁸F]THK-523

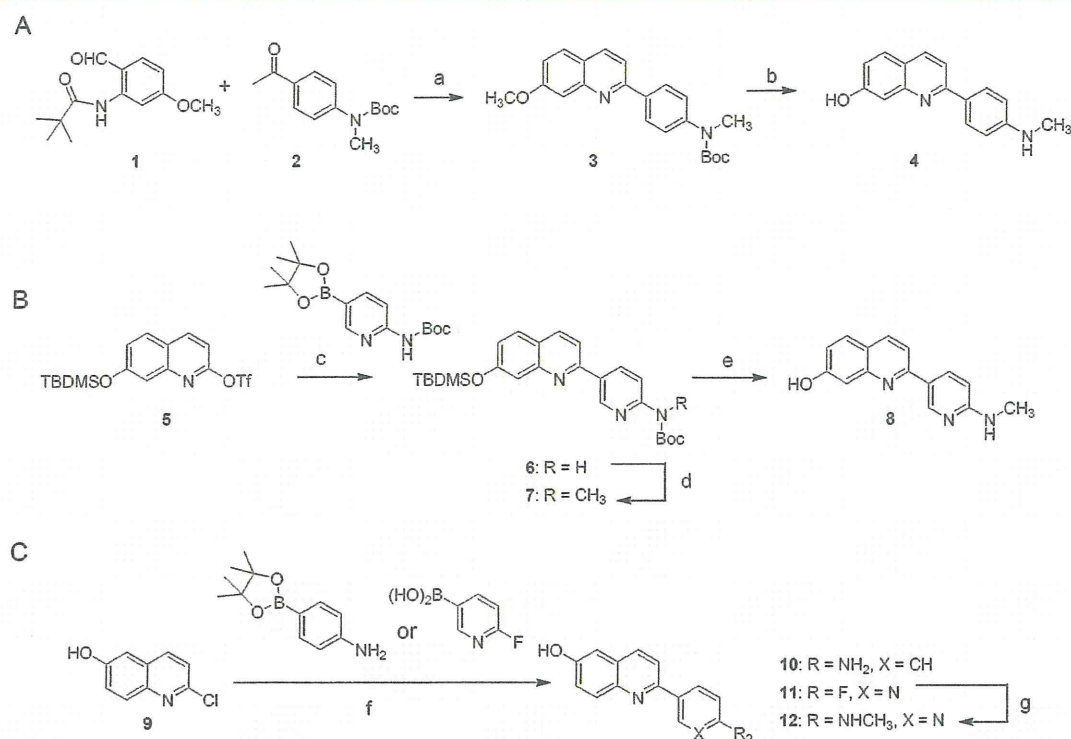
[¹⁸F]THK-523 was synthesized as described previously.²⁷ The product was formulated with DMSO. The specific activity of [¹⁸F]THK-523 was 121.7 GBq/ μ mol (end of synthesis), and the radiochemical purity was >99%. Competitive binding assay was performed as described previously²⁸ with [¹⁸F]THK-523 (final concentration: 4.1 nM) used as a radioligand of the assay.

Autoradiography of [¹¹C]THK-951

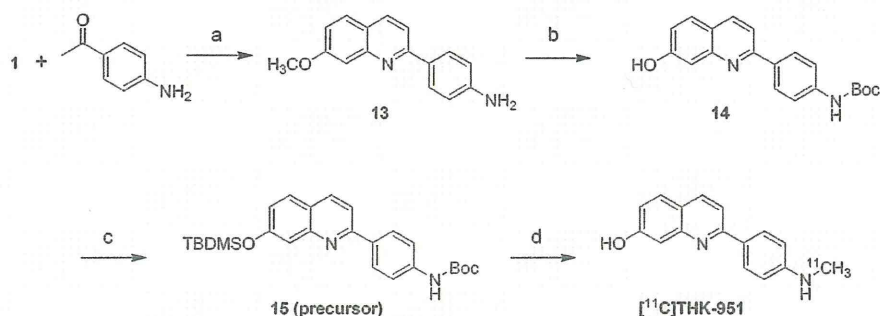
The hippocampal brain sections from a case of AD (82-year-old woman) were used for *in vitro* ARG. Deparaffinized sections were treated with a saline solution of [¹¹C]THK-951 (25% ethanol, 0.4 MBq/mL) or [¹⁸F]THK-523 (25% DMSO, 0.6 MBq/mL) for 10 min at room temperature. The sections were washed briefly with H₂O and 50% ethanol. After drying, the labeled sections were exposed to a BAS-III imaging plate (Fuji Film, Tokyo, Japan) for 3 h ([¹¹C]THK-951) or overnight ([¹⁸F]THK-523). Autoradiographic images were obtained using the BAS-5000 phosphor imaging instrument (Fuji Film). Adjacent brain sections were immunostained with anti-tau antibody (AT8; Innogenetics) and anti-A β antibody (6F/3D; Dako, Glostrup, Denmark).

Ex vivo biodistribution assay of [¹¹C]THK-951 in normal mice

Ex vivo biodistribution assay was performed as described previously.²⁸ Briefly, [¹¹C]THK-951 (saline solution: 1.8–1.9 MBq/200 μ L) was administered to male ICR mice (average weight: 29 g) via the tail vein. The mice were anesthetized with isoflurane and sacrificed by decapitation at 2, 10, 30, 60, and 90 min postinjection. The brain, blood, and other organs were excised.



Scheme 1. Synthesis of hydroxyquinoline derivatives (refer to Supporting Information). A: Synthesis of THK-951. (a) KHMOS, THF. (b) BBr₃, CH₂Cl₂. B: Synthesis of THK-953. (c) Na₂CO₃, Pd(PPh₃)₄, DME/H₂O. (d) CH₃I, NaH, DMF. (e) 1. TBAF, THF, 2. TFA, CH₂Cl₂. C: Synthesis of THK-5272 and THK-5273. (f) Na₂CO₃, Pd(PPh₃)₄, DME/H₂O/EtOH. (g) NH₂CH₃, MeOH.



Scheme 2. Synthesis of the precursor (refer to Supporting Information) and radiosynthesis of [¹¹C]THK-951. (a) 1. KHMOS, THF, 2. concentrated HCl, EtOH. (b) 1. BBr₃, CH₂Cl₂, 2. (Boc)₂O, NaHCO₃, THF/H₂O, 3. aqueous KOH, MeOH. (c) TBDMSCl, imidazole, DMF. (d) 1. [¹¹C]CH₃OTf, tBuOK, DMSO, 2. 2 N HCl.

After the organs were weighed, their radioactivity was counted with an automatic γ -counter. The percentage injected dose per gram (%ID/g) was calculated by comparing tissue counts to tissue weight. Each % ID/g value is an average of four separate experiments.

Results and discussion

Pittsburgh compound B, a representative β -amyloid probe for PET, is a 6-hydroxy substituted derivative of 2-arylbenzothiazole. Introduction of a hydroxyl group resulted in low lipophilicity of the probe and rapid clearance of free radioactivity from the brain.⁶ These characteristics are essential features for brain imaging probes because nonspecific signals interfere with quantitative analysis of PET images. Therefore, we focused on hydroxyl substituted BF-158 derivatives as tau imaging

probe candidates expecting they would provide appropriate brain kinetics.

The synthetic procedures of THK-951, THK-953, THK-5272, and THK-5273 are shown in Scheme 1 (details of the synthesis are described in the Supporting Information). THK-951 is a 2-phenylquinolin-7-ol derivative synthesized through a condensation reaction of two phenyl rings (Scheme 1A). The cyclocondensation of benzaldehyde (**1**) and acetophenone (**2**) in the presence of potassium *bis*(trimethylsilyl)amide gave **3**. THK-951 (**4**) was obtained by the deprotection of **3** by boron tribromide.

The THK-953 synthesis was outlined in Scheme 1B. **6** was obtained by Suzuki coupling between 7-hydroxyl-protected quinoline triflate (**5**) and pyridine boronic acid pinacol ester. After the *N*-methylation (**7**), deprotection of the TBDMS and Boc groups by treating with TBAF and TFA, respectively, gave THK-953 (**8**).

The 2-chloroquinolin-6-ol (**9**), which was prepared from quinolin-2,6-diol by selective chlorination, was used for the synthesis of the 6-hydroxy substituted 2-arylquinoline derivatives **10** (THK-5272) and **11** via Suzuki coupling reaction (Scheme 1C). THK-5273 (**12**) was obtained by a nucleophilic substitution reaction with methylamine from **11**.

To estimate the blood–brain barrier permeability of hydroxyquinoline derivatives, logP values were measured by an HPLC method and found to range from 0.5 to 1.3 (Table 1). These data indicated that the hydroxyquinoline derivatives have sufficient lipophilicity to penetrate the blood–brain barrier.²⁷

To evaluate the tau fibril binding characteristics of the synthesized hydroxyquinoline derivatives, we carried out fluorescence analyses (Figure 2). Fluorescence of the dye thioflavin-T or thioflavin-S increases when they bind to amyloid fibrils including fibrils from recombinant tau constructs.^{30,32} Similar to these dyes, BF-158 derivatives show enhanced fluorescence intensities upon binding to a cross β -sheet structure. The results from the fluorescence binding assays using recombinant K18 Δ 280K-tau fibrils indicated that the fluorescence enhancement of THK-951 and THK-5272 was observed in the presence of tau fibrils (Figure 2A, G). In contrast, the pyridine-containing derivatives, THK-953 and THK-5273, showed little change in fluorescence intensity or, interestingly, slightly weakening in the presence of tau fibrils (Figure 2D, J). The elaborate verification of the cause of this fluorescence change was not examined in the present study, but the possibility of a quenching effect caused by the binding conformation of the compounds is presumed.

Subsequently, fluorescent staining using AD hippocampal sections was performed to examine the in vitro binding affinity of the tested compounds for tau pathology in AD tissues. THK-951 clearly stained NFTs and neuropil threads in the hippocampal section of an AD brain under a blue filter (Figure 2B, C). THK-5272 also stained NFTs but with a lower contrast image compared with THK-951 (Figure 2E, F). The neuropathological staining with BF-170, which is a dehydroxylated derivative of THK-5272, showed high affinity for NFTs rather than SPs²⁶; thus, a contribution from the substituted position of the hydroxyl group to the affinity for NFTs was indicated. THK-953 (Figure 2H, I) and THK-5273 (Figure 2K, L) are highly fluorescent compounds, but very weak images of tau pathology were observed in this study. These results correlated with the results from the fluorescence binding assay using recombinant tau fibrils and indicated that the quinoline-pyridine derivatives bind very little to regions of tau pathology or have low binding affinity easily removable by a brief wash.

For further comparison of the binding affinity of hydroxyquinoline derivatives for recombinant tau fibrils, we determined their K_i values

in competition with [¹⁸F]THK-523, a tau imaging probe for PET. The K_i values of THK-951, THK-953, THK-5272, and THK-5273 were 20.7, 110.4, 36.1, and 30.4, respectively (Table 1). THK-951 had the highest affinity for tau fibrils from the hydroxyquinoline derivatives tested. In contrast with the image obtained for its fluorescent staining, THK-5273 showed comparable affinity with THK-5272. The weak staining of THK-5273 was probably caused by its high sensitivity to the washing technique used or the absence of a fluorescent hyperchromic effect compared with THK-5272.

In this study, the quinoline derivatives with higher lipophilicities had lower K_i values. For $A\beta$ ligands, it is considered that the lipophilicity of the ligand correlates with the degree of nonspecific binding but is not correlated with its binding affinity for $A\beta$ fibrils.^{6,33} It is possible that the lipophilicity of a compound has a considerable effect on its binding affinity for the cross β -sheet structures of tau; however, more structure–activity related studies are needed to understand this further.

Following the results of the fluorescence assays and competitive binding assay, we selected THK-951 for additional studies using a radiolabeled ligand, with consideration of the availability of THK-951 for a tau PET probe. Radiolabeling of THK-951 was performed using an *N*-Boc and *O*-TBDMS protected precursor (**15**) and [¹¹C]MeOTf (Scheme 2). [¹¹C]THK-951 was obtained in yields of 39% on average with radiochemical purity greater than 99% after HPLC purification. The average specific activity of [¹¹C]THK-951 was 83.2 GBq/ μ mol.

The poor brain kinetics of a PET tracer can harm the quantitative performance of a PET study, so high blood–brain barrier permeability and rapid clearance from the brain are essential for brain imaging agents. To evaluate the brain kinetics of [¹¹C]THK-951, we carried out an ex vivo biodistribution study using normal mice (Table 2). [¹¹C]THK-951 showed rapid brain uptake ($3.23 \pm 0.27\%$ ID/g at 2 min) and smooth washout from the normal brain ($0.11 \pm 0.01\%$ ID/g at 60 min), resulting to a high 2-min-to-60 min ratio (29.4) of brain uptake of [¹¹C]THK-951. This uptake ratio in a normal mouse brain is superior to that of [¹⁸F]THK-523 (1.86), [¹⁸F]THK-5105 (9.20), or [¹⁸F]THK-5117 (23.1),²⁸ indicating that our structural optimization worked as intended. Compared with these ¹⁸F-labeled tracers, the binding affinity of [¹¹C]THK-951 for tau aggregates is slightly lower, but the superiority in brain kinetics could make up for its weakness in binding affinity. It is known that the concentrations of tau aggregates are lower than those of $A\beta$ in an AD brain²²; therefore, a higher elimination efficiency of the free radiotracer from the brain would be more important for tau probes than for $A\beta$ probes. The fast clearance of [¹¹C]THK-951 from a normal mouse brain is likely caused by its low lipophilicity. The uptake in the kidney was highest at 2 min postinjection (19.8 % ID/g) followed by a fast clearance. The uptake in the liver showed a slow clearance after 10 min postinjection, while the radioactivity in the small intestine increased with time, indicating the biliary excretion of radioactive agents.

Finally, as an assessment of the binding affinity of [¹¹C]THK-951 for the regions of tau pathology, ARG analysis using AD hippocampal sections was performed. The ARG image showed high accumulation of [¹¹C]THK-951 in the CA1 region of the AD hippocampus (Figure 3A). Distribution of the tracer signal of [¹¹C]THK-951 correlated well with that of [¹⁸F]THK-523 (Figure 3B) and tau immunostaining (Figure 3C). On the other hand, the distribution of the tracer signal was different from the immunostained $A\beta$ pathology, which showed spotty distribution in that region (Figure 3D).

Table 1. Lipophilicity (logP) and binding affinity (K_i values) of hydroxyquinoline derivatives to recombinant tau fibrils

Compound name	X	R ₁	R ₂	logP*	K_i (nM)
THK-951	C	NHCH ₃	7-OH	1.28	20.7
THK-953	N	NHCH ₃	7-OH	0.56	110.4
THK-5272	C	NH ₂	6-OH	0.61	36.1
THK-5273	N	NHCH ₃	6-OH	0.90	30.4

*logP values were determined by HPLC method.

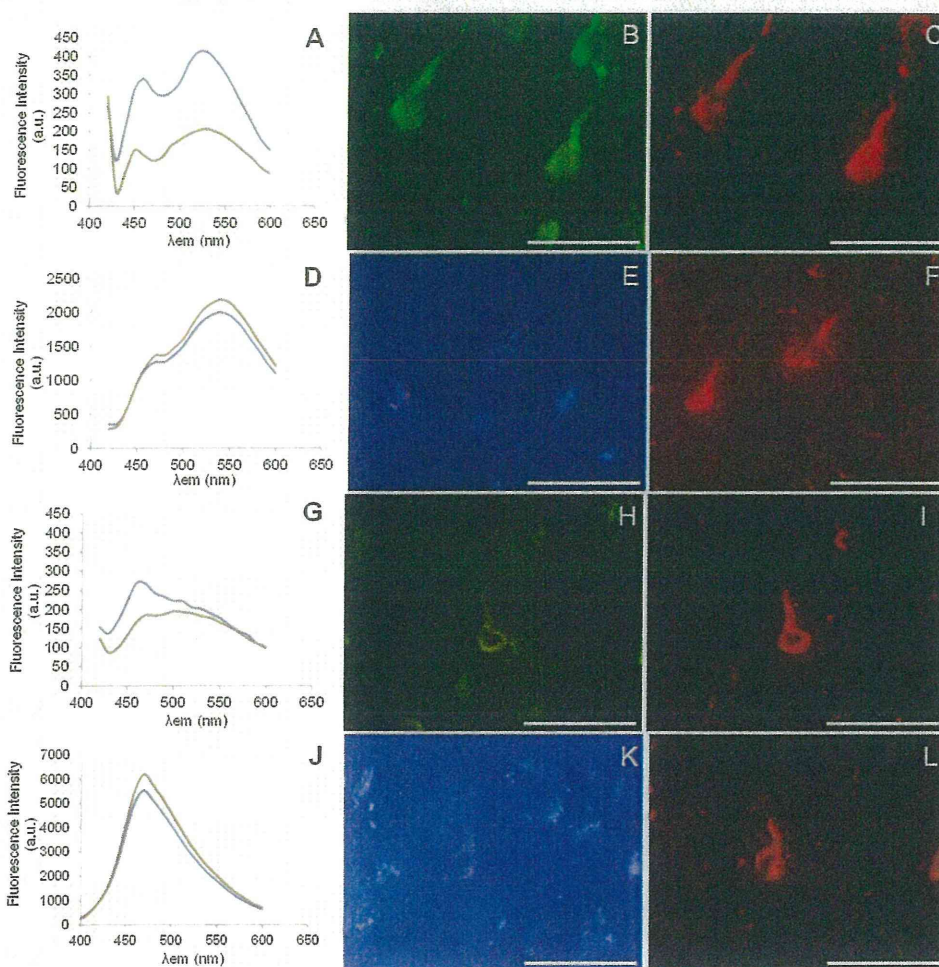


Figure 2. Fluorescence spectral analyses and neuropathological staining of THK-951 (A–C), THK-953 (D–F), THK-5272 (G–I), and THK-5273 (J–L). (A, D, G, and J) Fluorescence spectra of THK-951 (A, $\lambda_{\text{ex}} = 390$ nm), THK-953 (D, $\lambda_{\text{ex}} = 390$ nm), THK-5272 (G, $\lambda_{\text{ex}} = 390$ nm), and THK-5273 (J, $\lambda_{\text{ex}} = 360$ nm) in the presence or absence of K18 Δ 280K-tau fibrils (K18 Δ 280K-tau: blue lines; control (ligands only): red lines). (B, C, E, F, H, I, K, and L) Double staining with hydroxyquinoline derivatives and anti-pTau antibody (AT8). (B, E, H, and I) Fluorescent staining of hippocampal sections from cases of Alzheimer's disease (THK-951: B; THK-953: E; THK-5272: H; THK-5273: K). (C, F, I, and L) Immunostaining by AT8. Scale bars: 50 μm . This figure is available in color online at wileyonlinelibrary.com/journal/jlcr

Table 2. Biodistribution of [^{11}C]THK-951 in ICR mice

Tissue	2 min	10 min	30 min	60 min	90 min
Blood	2.65 (0.46)	1.20 (0.48)	0.20 (0.04)	0.12 (0.01)	0.11 (0.02)
Brain	3.23 (0.27)	0.81 (0.13)	0.15 (0.05)	0.11 (0.01)	0.06 (0.01)
Liver	10.14 (2.66)	10.00 (1.79)	1.99 (0.45)	1.10 (0.23)	0.85 (0.27)
Kidney	19.79 (6.77)	4.10 (0.34)	0.96 (0.43)	0.49 (0.11)	0.35 (0.09)
Small intestine	4.72 (1.44)	12.22 (3.10)	24.91 (3.17)	29.33 (2.23)	24.64 (1.83)

Data are expressed as mean of % ID/g (Standard Deviation) ($n = 4$).

These results indicated that [^{11}C]THK-951 was promising in its ability to bind regions of tau pathology in the AD brain.

In vivo tau imaging will allow the accurate measurement of the distribution of tau pathology in the AD brain. The combined

assessments of tau burden and other biomarkers of AD (e.g., A β burden, brain metabolism, and clinical findings) are needed to understand the accurate pathogenic mechanism or time course of AD.⁴ One of the advantages of developing ^{11}C -labeled tau probes is that tau probes labeled with this short-half-life radionuclide will facilitate two PET studies in the same day by using other PET probes such as [^{18}F]FDG or A β PET after the tau imaging.

To develop probes with ideal brain kinetics, we introduced a hydroxyl group at the 6 or 7 position of quinoline. Lipophilicity has considerable influences on not only tracer kinetics but also binding affinity; therefore, lipophilicity needs to be optimized for tau tracers. In this study, the properties of [^{11}C]THK-951 ($\log P = 1.28$) were balanced between achieving high binding affinity for tau fibrils and blood–brain permeability with a fast clearance from mouse brain. We plan to evaluate other derivatives having different hydroxylated positions or alkyl amino groups to obtain additional structure–activity relationship information.

A competitive binding assay using a radiolabeled ligand may ensure the examination of tau binding ligands, which do not seem to have binding affinity for tau pathology in a fluorescence

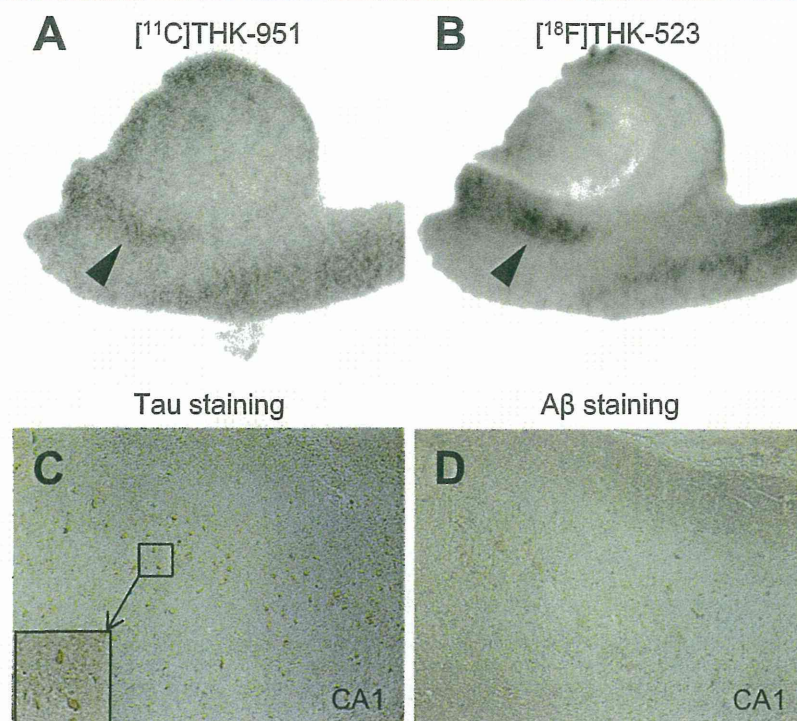


Figure 3. Characterization of in vitro binding of [^{11}C]THK-951 to tau pathology by autoradiography and immunohistochemistry. [^{11}C]THK-951 showed high accumulation in the hippocampal CA1 region (A, filled arrowhead). Similarly, [^{18}F]THK-523, a well-characterized tau probe, also highly accumulated in the CA1 region (B, filled arrowhead). Immunostaining of adjacent sections demonstrated that numerous tau immunopositive neurofibrillary tangles were observed in CA1 region (C). By contrast, A β staining showed weak immunoreactivity in CA1 region (D).

binding assay using AD brain sections. On the other hand, some researchers indicated that the PHFs constructed from tau fragments do not fully conform to the structure of PHFs from an AD brain.^{22,32} Thus, these in vitro binding assay results should be considered carefully, and comparison with the results from future clinical studies would facilitate our selection of an evaluation method.

Conclusion

We synthesized four hydroxyquinoline derivatives and performed biological evaluations to estimate their potential as tau imaging probes. From these results, we selected THK-951 for additional studies and successfully radiosynthesized [^{11}C]THK-951. [^{11}C]THK-951 showed ideal brain kinetics in normal mice, and its binding affinity for regions of tau pathology was confirmed by an in vitro ARG assay using AD hippocampal sections. Further evaluation of THK-951 and structurally optimized derivatives will facilitate our understanding about AD tau pathology in the living body.

Acknowledgements

This study was supported by the Industrial Technology Research Grant Program of the NEDO (09E51025a) in Japan, the Health and Labour Sciences Research Grants from the Ministry of Health, Labour, and Welfare of Japan, Grant-in-Aid for Scientific Research (B) (23390297), and the 'Japan Advanced Molecular Imaging Program (J-AMP)' of the Ministry of Education, Culture, Sports, Science, and Technology of Japan.

Conflict of Interest

This study was supported by the research fund from GE Healthcare.

References

- [1] K. Ogomori, T. Kitamoto, J. Tateishi, Y. Sato, M. Suetsugu, M. Abe, *Am. J. Pathol.* **1989**, *134*, 243–51.
- [2] H. Braak, E. Braak, *Acta Neuropathol.* **1991**, *82*, 239–59.
- [3] P. M. Thompson, K. M. Hayashi, G. de Zubicaray, A. L. Janke, S. E. Rose, J. Semple, D. Herman, M. S. Hong, S. S. Dittmer, D. M. Doddrell, A. W. Toga, *J. Neurosci.* **2003**, *23*, 994–1005.
- [4] C. R. Jack, D. S. Knopman, W. J. Jagust, R. C. Petersen, M. W. Weiner, P. S. Aisen, L. M. Shaw, P. Vemuri, H. J. Wiste, S. D. Weigand, T. G. Lesnick, V. S. Pankratz, M. C. Donohue, J. Q. Trojanowski, *Lancet Neurol.* **2013**, *12*, 207–16.
- [5] E. D. Agdeppa, V. Kepe, J. Liu, S. Flores-torres, N. Satyamurthy, A. Petric, G. M. Cole, G. W. Small, S. Huang, J. R. Barrio, *J. Neurosci.* **2001**, *21*, 1–5.
- [6] C. A. Mathis, Y. Wang, D. P. Holt, G. Huang, M. L. Debnath, W. E. Klunk, *J. Med. Chem.* **2003**, *46*, 2740–2754.
- [7] S. R. Choi, G. Golding, Z. Zhuang, W. Zhang, N. Lim, F. Hefti, T. E. Benedum, M. R. Kilbourn, D. Skovronsky, H. F. Kung, *J. Nucl. Med.* **2009**, *50*, 1887–94.
- [8] Y. Kudo, N. Okamura, S. Furumoto, M. Tashiro, K. Furukawa, M. Maruyama, M. Itoh, R. Iwata, K. Yanai, H. Arai, *J. Nucl. Med.* **2007**, *48*, 553–561.
- [9] M.-P. Kung, C. Hou, Z.-P. Zhuang, B. Zhang, D. Skovronsky, J. Q. Trojanowski, V. M.-Y. Lee, H. F. Kung, *Brain res.* **2002**, *956*, 202–10.
- [10] M. M. Svedberg, O. Rahman, H. Hall, *Nucl. Med. Biol.* **2012**, *39*, 484–501.
- [11] V. L. Villemagne, K. E. Pike, D. Darby, P. Maruff, G. Savage, S. Ng, U. Ackermann, T. F. Cowie, J. Currie, S. G. Chan, G. Jones, H. Tochon-Danguy, G. O'Keefe, C. L. Masters, C. C. Rowe, *Neuropsychologia* **2008**, *46*, 1688–97.